New Insights in the Ontogeny and Taphonomy of the Devonian Acanthodian Triazeugacanthus affinis From the Miguasha Fossil-Lagerstätte, Eastern Canada

Marion Chevrinais, Etienne Balan, Richard Cloutier

minerals

MDPI

Article

New Insights in the Ontogeny and Taphonomy of the Devonian Acanthodian *Triazeugacanthus affinis* From the Miguasha *Fossil-Lagerstätte*, Eastern Canada

Marion Chevrinais [1], Etienne Balan [2] and Richard Cloutier [1,*]

Received: 28 October 2015; Accepted: 16 December 2015; Published: 23 December 2015
Academic Editors: Karim Benzerara, Jennyfer Miot and Thibaud Coradin

[1] Département de Biologie, Chimie et Géographie, Université du Québec à Rimouski, Rimouski, QC G5L 3A1, Canada; marion.chevrinais@uqar.ca
[2] Institut de Minéralogie, de Physique des Matériaux et de Cosmochimie, Sorbonne Universités, UPMC Univ Paris 06, CNRS UMR 7590, IRD UMR 206, MNHN, F-75005 Paris, France; Etienne.Balan@impmc.jussieu.fr
* Correspondence: richard_cloutier@uqar.ca; Tel.: +1-418-723-1986 (ext. 1771)

Abstract: Progressive biomineralization of a skeleton occurs during ontogeny in most animals. In fishes, larvae are poorly mineralized, whereas juveniles and adults display a progressively more biomineralized skeleton. Fossil remains primarily consist of adult specimens because the fossilization of poorly-mineralized larvae and juveniles necessitates exceptional conditions. The Miguasha *Fossil-Lagerstätte* is renowned for its Late Devonian vertebrate fauna, revealing the exceptional preservation of fossilized ontogenies for 14 of the 20 fish species from this locality. The mineralization of anatomical structures of the acanthodian *Triazeugacanthus affinis* from Miguasha are compared among larval, juvenile and adult specimens using Energy Dispersive X-ray Spectrometry. Chemical composition of anatomical structures of *Triazeugacanthus* reveals differences between cartilage and bone. Although the histology and anatomy is well-preserved, Fourier transform infrared spectrometry shows that the original chemical composition of bone is altered by diagenesis; the mineral phase of the bone (*i.e.*, hydroxyapatite) is modified chemically to form more stable carbonate-fluorapatite. Fluorination occurring in mineralized skeletal structures of adult *Triazeugacanthus* is indicative of exchanges between groundwater and skeleton at burial, whereas the preservation of larval soft tissues is likely owing to a rapid burial under anoxic conditions. The exceptional state of preservation of a fossilized ontogeny allowed us to characterize chemically the progressive mineralization of the skeleton in a Devonian early vertebrate.

Keywords: Acanthodii; biomineralization; fossilized ontogeny; paleontology; Devonian

1. Introduction

Fossilized fish ontogenies are rare, especially in the Paleozoic [1] because the mineralization of an animal's skeleton progresses during ontogeny and the preservation of poorly mineralized or ossified structures of immature (larval and juvenile) specimens requires exceptional fossilization conditions. Biomineralization of the skeleton during ontogeny is a condition shared by most vertebrates [2]. Extant jawless fish (hagfishes and lampreys) lack biomineralized tissues, which differs from their extinct relatives [1,2]. In extant cartilaginous fishes (Chondrichthyes; chimaera, sharks, skates and rays), the skeleton mineralizes as ontogeny progresses, at least superficially by means of tesserate calcified cartilage [3,4]. In extant bony fishes (piscine Osteichthyes; ray-finned fishes, coelacanths and dipnoans), young individuals show an unmineralized or poorly mineralized skeleton whereas older ones are highly mineralized [5–7]. In extinct jawed vertebrates, such as acanthodians and

placoderms, this progressive biomineralization is assumed, rather than observed, because of the rarity of ontogenetic material but also because fossilization processes tend to favor the preservation of hard tissues, thus, frequently leaving an information gap during early ontogenetic stages. Since ontogenies have the potential to elucidate evolutionary developmental patterns and processes from the deep past [1,8], it is crucial to detect if fossilization biased our understanding of the early phase of biomineralization and how it could modify the preservation of the original tissues in fossils.

Vertebrate fossils predominantly consist of remains of mineralized skeletal structures [9], while soft tissues are only preserved exceptionally [10–13]. The quality and fidelity of tissue preservation depend, among other things, on the nature of the tissues in the organism, the amount of decay that precedes mineralization, and the availability of mineral-forming ions. It is however often difficult to determine whether the minerals observed in the fossils correspond to the original biomineralization of the tissues or result from diagenetic transformations of the fossils [14]. The comparison of chemical and mineralogical composition of anatomical structures during the ontogeny of an organism allows one to discriminate between these two mineralization processes. Indeed, as the biomineralization of skeletal structures progresses during ontogeny, or in relation to the size of an individual, the chemical and mineralogical signatures of skeletal structures change (e.g., carbon or calcium phosphate composition for cartilage or bone, respectively) [15,16]. On the other hand, an increase in exogenous ions (e.g., F ions) and modifications of the internal structure of skeletal tissues are expected with diagenetic mineralization, because it likely depends on local fossilization conditions.

The rapidity of consumption (*i.e.*, mechanical degradation by predators or scavengers) and decay (*i.e.*, degradation by bacteria) of an animal under oxic conditions is negatively correlated with the preservation of soft tissues in an aquatic environment [17]. The decomposition process of organic carbon by aerobic respiration roughly corresponds to the transformation of organic and dioxygen molecules into carbon dioxide and water molecules. Thus, anoxic conditions can be reached when the amount of organic carbon exceeds the oxygen supply. Specifically, the deposition of a large number of individuals (mass mortality) during a short period of time can locally reduce the level of dissolved oxygen which could create anoxic condition at the water/sediment boundary, decreasing scavenging and bioturbation [17]. These sporadic mass mortality events are characterized by a large number of fossil specimens in a given horizon. Fossiliferous sites and horizons yielding assemblages of mass mortalities are qualified as *Konzentrat-Lagerstätten*. Furthermore, when these fossiliferous environments present exceptionally well-preserved specimens, they are qualified of *Konservat-Lagerstätten*. It is likely that both, *Konzentrat-* and *Konservat-Lagerstätten*, favor soft tissues preservation.

Skeletal tissues showing early phases of biomineralization are prompt to be affected by two fossilization processes: the permineralization and the authigenic mineralization. Permineralization results from the early infiltration and permeation of tissues by mineralizing aqueous solutions [18]. In contrast, authigenic mineralization is often a product of biological tissues decay by bacterial activity; therefore, the types of minerals depend on the chemical composition of the sediment and the environmental conditions when bacterial decay occurred [19].

The Late Devonian Miguasha *Fossil-Lagerstätte* (Québec City, QC, Canada), a United Nations Educational, Scientific and Cultural Organization (UNESCO) World Heritage Site, yielded fossilized ontogenies for 14 out of the 20 fish species [20]. Among these 14 species, larval and juvenile specimens of the acanthodian *Triazeugacanthus affinis* have been reinterpreted recently [21]. The exceptional preservation of a large number of *Triazeugacanthus* within a large size range allowed the description of ontogenetic changes. This ontogenetic series is characterized by the simultaneous increase in the number of skeletal structures and the progressive extension of the squamation as a function of animal size [21]; thus, endoskeletal as well as exoskeletal mineralization proceed simultaneously.

In the present study, our main objectives are (1) to compare the chemical and mineralogical composition of larval, juvenile and adult specimens of *Triazeugacanthus*; and (2) to provide new information about the diagenesis of *Triazeugacanthus* from the Miguasha *Fossil-Lagerstätte*.

2. Experimental Section

2.1. Materials

The acanthodian *Triazeugacanthus affinis* Whiteaves, 1887 is common (more than 300 complete or almost complete specimens) in the middle Frasnian Escuminac Formation (Miguasha, QC, Canada) [22]. The distribution of *Triazeugacanthus* is uneven lithologically and stratigraphically. *Triazeugacanthus* is found predominantly in the laminites [22] and occurs primarily in two stratigraphic zones of the Escuminac Formation (*i.e.*, from 5 to 17 m and from 83 to 90 m from the base of the Escuminac Formation (Richard Cloutier, personal observation).

Three ontogenetic stages (larval, juvenile and adult) have been recognized in *Triazeugacanthus* based on the degree of squamation, the progression of the ossification and the size of the specimens [21]. Six complete or almost complete specimens, two larvae (Figure 1a–f), two juveniles (Figure 1j–o, and Figure 2a–f) and two adults (Figure 2h–s) and one thin section of the dermal skeleton of a juvenile (Figure 1g–i) *Triazeugacanthus* preserved in laminites, have been used for the non-destructive scanning electron microscopy (SEM) coupled to the energy dispersive X-ray spectrometry (EDX) (Figures 1 and 2). One partial adult specimen of *Triazeugacanthus* allowing destructive analysis has been used for Fourier transform infrared spectrometry (FTIR) and X-ray diffraction (XRD) (Electronic Supplementary Material Figure S1). Specimens are curated in the Musée d'Histoire naturelle de Miguasha (MHNM) (Nouvelle, QC, Canada).

For comparison we used juveniles of two extant species: the black dogfish, *Centroscyllium fabricii* (Chondrichthyes) and the Atlantic mackerel, *Scomber scombrus* (Osteichthyes). Specimens were frozen and stored at −20 °C. Specimens were thawed, dissected and dried in an oven at 35 °C for 72 h before EDX analyses. A series of anatomical structures were analyzed with EDX for both species: Meckel's cartilage, palatoquadrate, eye lenses, and vertebral centra of *C. fabricii* (Electronic Supplementary Material Figure S2); exoccipital, dentary, basihyal and eye lenses of *S. scombrus* (Electronic Supplementary Material Figure S3).

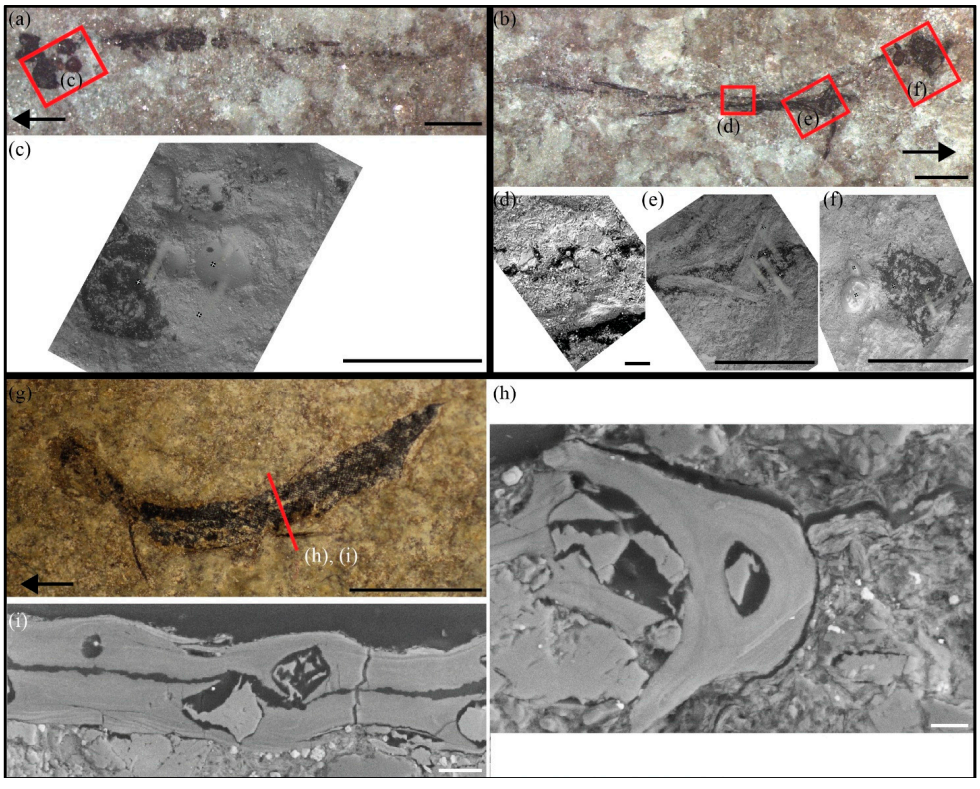

Figure 1. *Cont.*

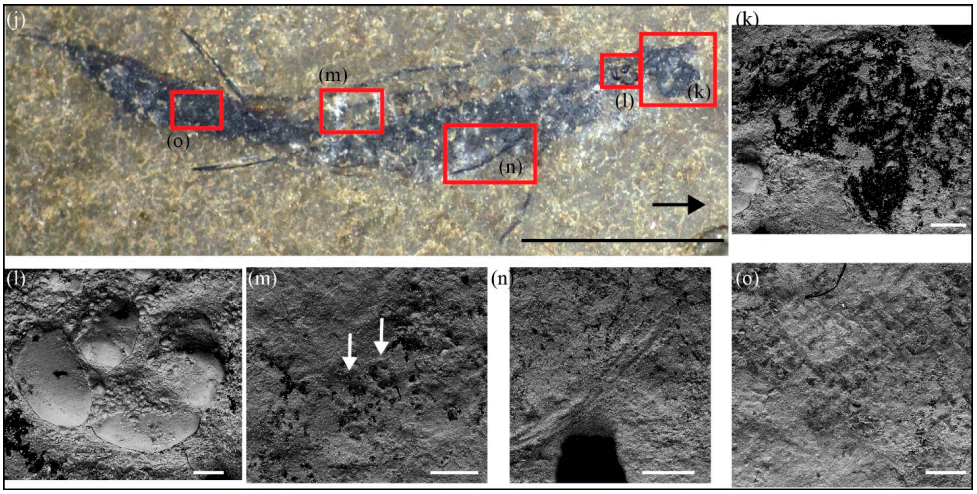

Figure 1. *Triazeugacanthus affinis* anatomical structures for energy dispersive X-ray spectrometry (EDX) analyses. (**a**) Larval specimen the Musée d'Histoire naturelle de Miguasha (MHNM) 03-440 #1 and scanning electron microscopy (SEM) close-ups of the (**c**) head region. (**b**) Larval specimen MHNM 01-440 #2 and SEM close-up of the (**d**) notochordal elements, (**e**) scapulocoracoid and pectoral fin spine, and (**f**) head region. (**g**) Juvenile specimen MHNM 03-398, red line shows the position of the histological section (**h**) of the anal spine and (**i**) the two lateral coverings of body scales in cross-sections. (**j**) Juvenile specimen MHNM 03-1252 and SEM close-ups of the (**k**) eye lenses, (**l**) otoliths, (**m**) notochordal elements (white arrows), (**n**) pectoral fin spine, (**o**) scales. Red squares show SEM close-up areas. Arrows point forward. Scale bars = 1 mm in (a) and (b); 600 μm in (c); 500 μm in (d); 800 μm in (e) and (f); 5 mm in (g) and (j); 10 μm in (h); 20 μm in (i); 200 μm in (k), (m), and (o); 100 μm in (l); and 500 μm in (n).

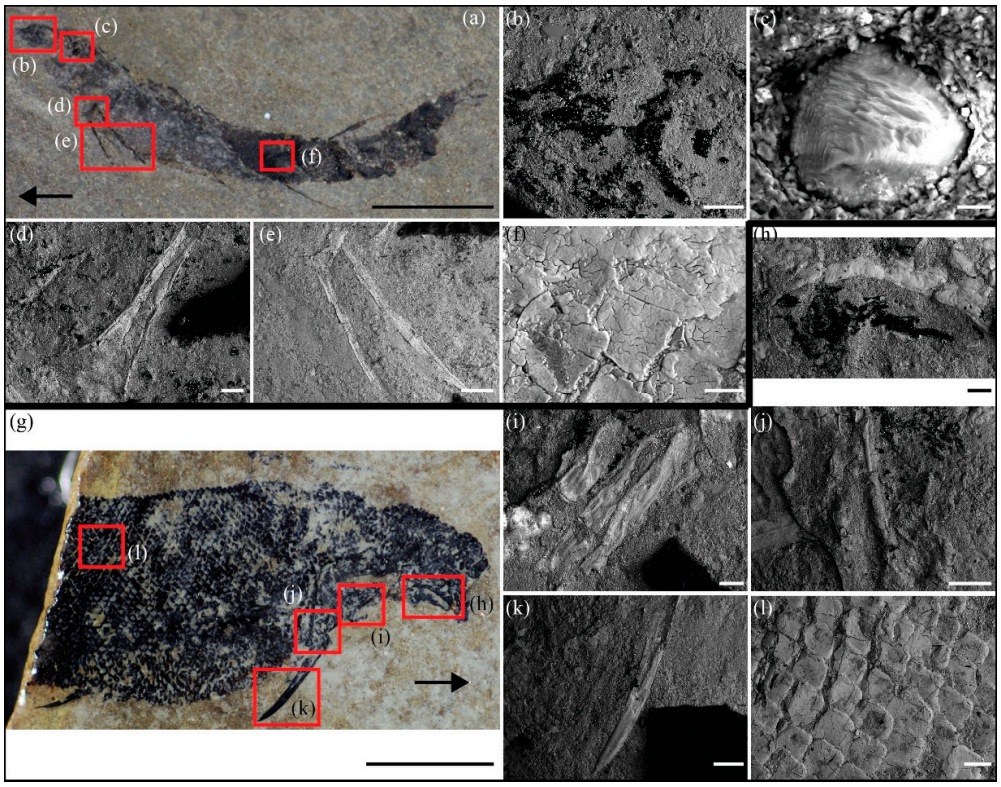

Figure 2. *Cont.*

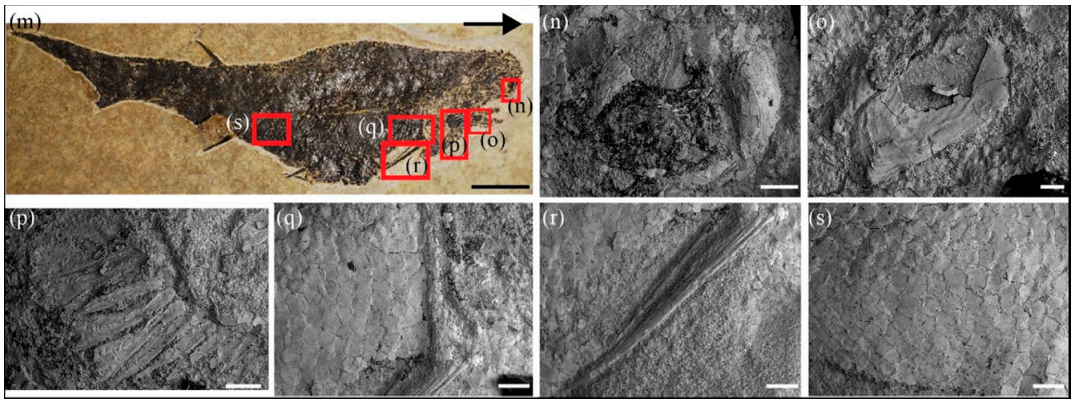

Figure 2. *Triazeugacanthus affinis* anatomical structures for EDX analyses. (**a**) Juvenile specimen MHNM 03-2684 and SEM close-ups of the (**b**) eye lenses, (**c**) otolith, (**d**) scapulocoracoid, (**e**) pectoral spines, and (**f**) scales. (**g**) Adult specimen MHNM 03-2669 and SEM close-ups of the (**h**) eye lenses and sclerotic plates, (**i**) branchiostegal rays, (**j**) scapulocoracoid, (**k**) pectoral fin spine and (**l**) scales. (**m**) Adult specimen MHNM 03-1497 and SEM close-ups of the (**n**) sclerotic plates, (**o**) palatoquadrate process, (**p**) branchiostegal rays, (**q**) scapulocoracoid, (**r**) pectoral fin spine and (**s**) scales. Red squares show SEM close-up areas. Arrows point forward. Scale bars = 5 mm in (a), (g) and (m); 200 µm in (b) and (h), 10 µm in (c), 100 µm in (d), (i), (o); 500 µm in (e), (j), (k), (n), (p), (q), (r), (s); 50 µm in (f).

2.2. Scanning Electron Microscopy (SEM) Observation and Energy Dispersive X-Ray Spectrometry (EDX) Analysis

SEM microscopy has been performed using an environmental JEOL 6460LV SEM (JEOL USA, Peabody, MA, USA). The surface of samples was observed without conductive coating. Elemental composition analysis was performed using an INCA X-sight (Oxford Instruments, Austin, TX, USA) energy dispersive X-ray spectrometer; this analysis permits to identify the presence of chemical elements in the skeletal structures [23,24]. Each spectrum was acquired with a 10-µm spot size, for 100 s of lifetime (process time 5, spectrum range 0–20 keV, 2000 channels) at an accelerating voltage of 20 kV. The detection limits of chemical elements are about 1000 ppm or 0.1 wt %. System quantitative optimization was done using Cu as a standard.

2.3. Fourier Transform Infrared Spectrometry

The surface of one adult specimen of *Triazeugacanthus* (MHNM 03-1699; Electronic Supplementary Material Figure S1) was scraped using a needle in order to obtain powder for Fourier transform infrared spectrometry (FTIR). Pellets for FTIR measurements were obtained by pressing a mixture of ~1.0 mg of gently ground sample diluted in 210 mg of dried KBr. Transmission IR spectra were recorded between 400 and 4000 cm^{-1}, by averaging 150 scans with a resolution of 1 cm^{-1}, using a Nicolet 6700 FTIR spectrometer (Thermo Fisher Scientific Inc., Waltham, MA, USA). The spectrometer was equipped with an Ever-Glo source, KBr beamsplitter and DTGS-KBr detector. The usual crystallinity index was calculated as the infrared splitting factor (IRSF): IRSF = (A605 + A565)/A590, where Ax is the measured absorbance at wavenumber x, assuming a straight baseline between 450 and 750 cm^{-1} [25,26].

2.4. X-Ray Diffraction

The mineralogical composition of the sedimentary rock was determined by powder X-ray diffraction (XRD) using a few mg of a sample obtained from the laminated matrix of *Triazeugacanthus* specimen MHNM 03-1699 (Electronic Supplementary Material Figure S1). The powder sample was deposited on a Si spinning sample holder. Analyses were performed using a PANALYTICAL® X'pert

Pro apparatus (PANalytical, Almelo, The Netherlands) using the Co Kα radiation. Measurements were performed from 2° to 90° in 1000 s with a fixed slit size of 1°.

3. Results

3.1. SEM Observations and EDX Analyses of Skeletal Tissues

3.1.1. Fossilized Tissues of *Triazeugacanthus affinis*

Chemical analyses of non-bony (eye lenses, otoliths), endochondral (palatoquadrate, scapulocoracoid, notochordal elements) and dermal elements (sclerotic plates, branchiostegal rays, pectoral spines, scales) have been performed for each ontogenetic stage (larval (Figure 3), juvenile (Figure 4) and adult (Figure 5)). Irrespective to the ontogenetic stages, (1) C and O are recorded in each skeletal element, (2) Ca and P are recorded in all dermal elements, and (3) the simultaneous presence of Ca and P is associated with F (with the exception of analyses performed on the internal structure of bones). Minor Al and Si contributions are detected and are likely related to the presence of aluminous clay minerals in the surrounding matrix (*i.e.*, illite and chlorite; Figures 3–5).

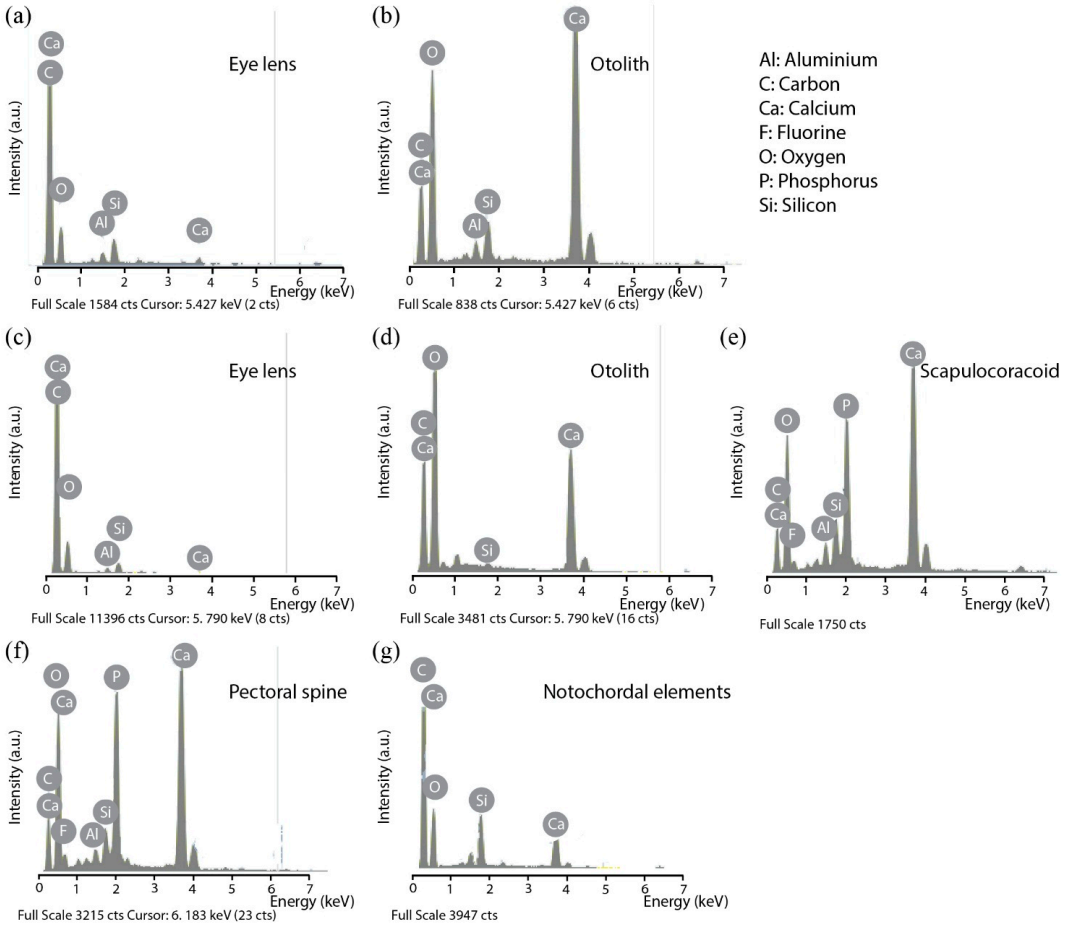

Figure 3. Representative spectra of larval *Triazeugacanthus* samples using EDX punctual microanalysis. (**a**) and (**b**) MHNM 03-440 #1. (**c**)–(**g**) MHNM 03-440 #2. Note that the intensity of the oxygen peak is non-significant and depends essentially on the vacuum level in the chamber of the environmental SEM.

In larval *Triazeugacanthus* (Figure 1a,b), notochordal elements and eye lenses are among the first elements to develop ([21]: Electronic Supplementary Material, Figure S3). Notochordal elements and eye lenses display C and O peaks with a minor contribution of Ca, Al and Si in the EDX

spectrum (Figure 3a,c,g). The notochordal elements (visible only in rare specimens) show no sign of mineralization (Figure 3g). During the larval stage, otoliths form shortly after the previous elements ([21]: Electronic Supplementary Material, Figure S3). These non-bony elements display a strong Ca peak and lack P; these results are consistent with the expected calcium carbonate composition [27] (Figures 1c,f and 3b,d). Among the first appendicular elements to form ([21]: Electronic Supplementary Material, Figure S3), the scapulocoracoid and the pectoral spine display clear Ca and P peaks associated to a F peak (Figures 1e and 3e,f). Even in the youngest occurrence of the scapulocoracoid (MHNM 03-440 #2; [21]: Electronic Supplementary Material, Figure S3), there is already a clear mineralized signature (Figure 3e); the pre-mineralized state of this endochondral element has not been sampled.

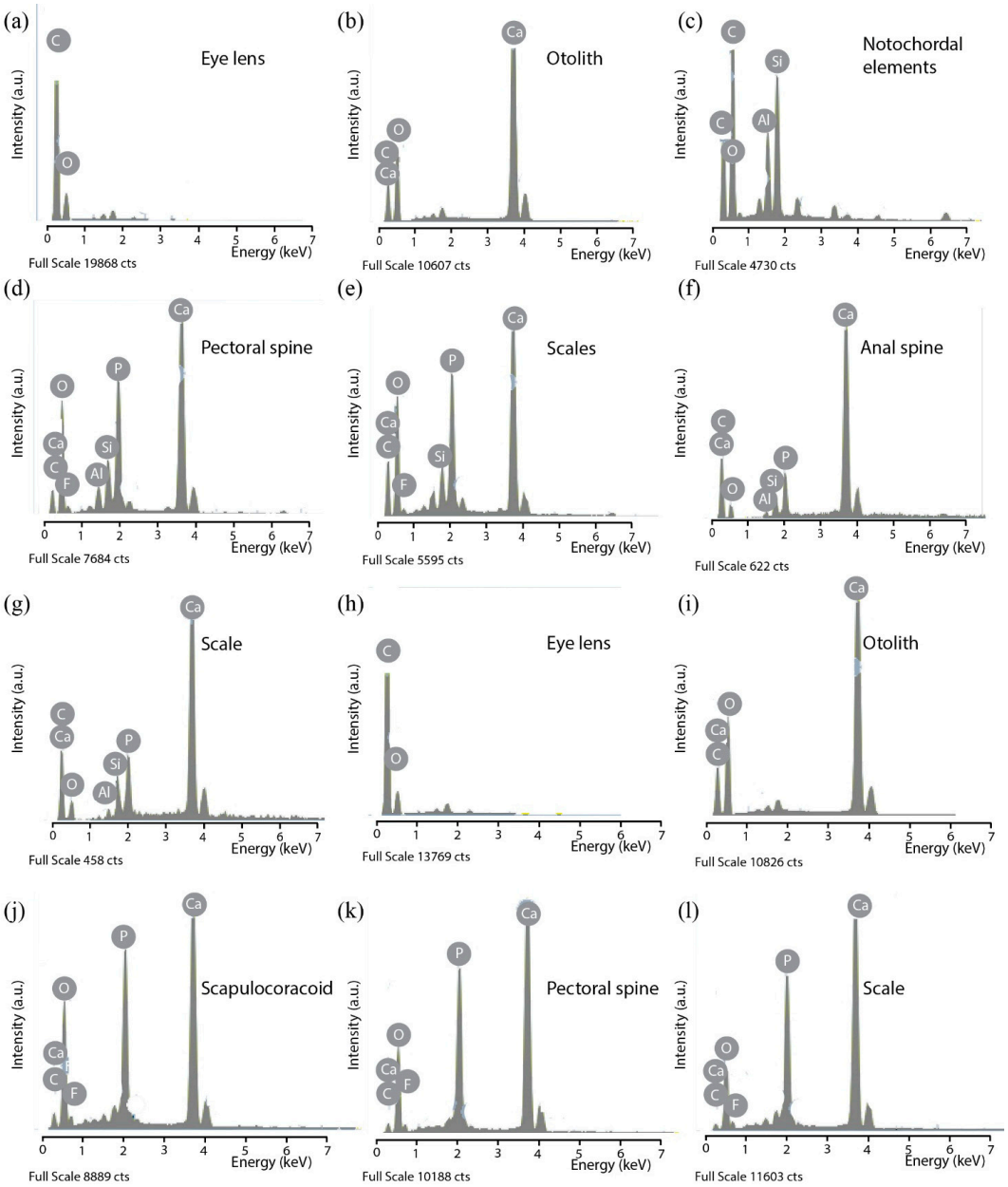

Figure 4. Representative spectra of juvenile *Triazeugacanthus* samples using EDX punctual microanalysis. (**a**)–(**e**) MHNM 03-1252. (**f**), (**g**) MHNM 03-398. (**h**)–(**l**) MHNM 03-2684. Note that the intensity of the oxygen peak is non-significant and depends essentially on the vacuum level in the chamber of the environmental SEM. See Figure 3 for chemical elements legend.

Juvenile *Triazeugacanthus* specimens (Figures 1j and 2a), characterized by the appearance and progression of the squamation [21], show dermal elements (scales: Figure 4e,g,l; spines: Figure 4d,f,k) with clear signatures of mineralization (Ca and P peaks). Elemental composition on the internal structure of dermal scales and spine (thin section; Figure 1h,i) also reveals the presence of Ca and minor P (Figure 4f,g), but the absence of F. Chemical composition of the eye lenses (Figure 4a,h), notochordal elements (Figure 4c), scapulocoracoid (Figure 4j) and otoliths (Figure 4b,i) remain similar to the larval condition.

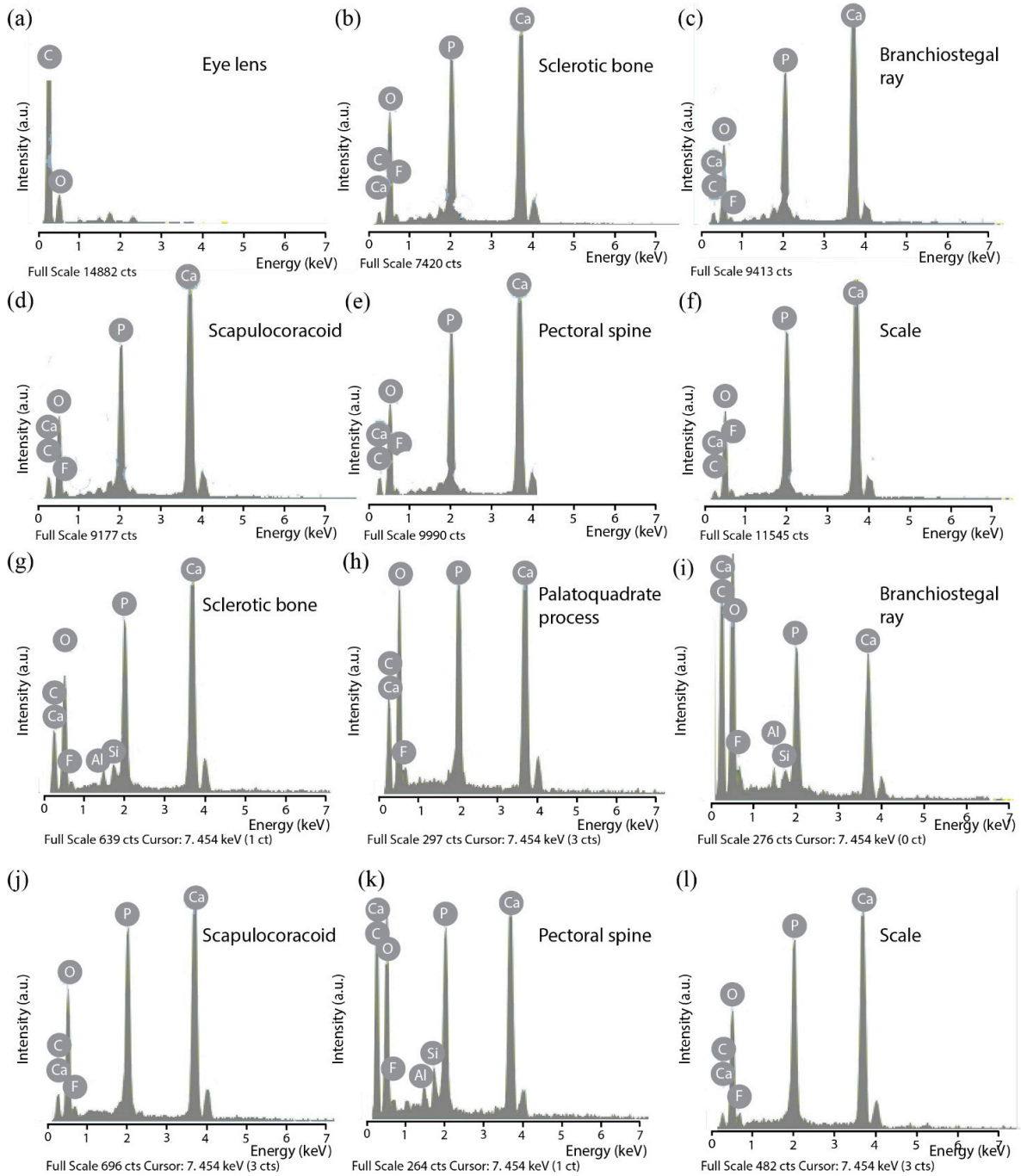

Figure 5. Representative spectra of adult *Triazeugacanthus* samples using EDX punctual microanalysis. (**a**)–(**f**) MHNM 03-2669. (**g**)–(**l**) MHNM 03-1497. Note that the intensity of the oxygen peak is non-significant and depends essentially on the vacuum level in the chamber of the environmental SEM. See Figure 3 for chemical elements legend.

In adult *Triazeugacanthus* specimens (Figure 2g,m), the chemical composition of previously formed skeletal structures remains similar to that of the immatures (Figure 5). The newly developed palatoquadrate (Figure 5h) is already mineralized. The dermal sclerotic plates (Figure 5b,g) and branchiostegal rays (Figure 5c,i) are also mineralized as suggested by the presence of strong Ca and P peaks (with similar relative intensities) associated with a F peak. Notochordal elements and otoliths are not observed in adults because they are overlaid by body and head scales, respectively.

3.1.2. Living Models: *Centroscyllium fabricii* and *Scomber scombrus*

The elemental composition analysis of the juvenile *C. fabricii* mostly consists in C, O and N, consistent with the absence of mineralization on the surface of the neurocranium, the eye lenses and the vertebral centra (Electronic Supplementary Material Figure S4). Tesserate mineralization indicated by the presence of P and Ca occurs in the mandibular and hyoid arches (Electronic Supplementary Material Figure S4). The skeletal structures of the juvenile *S. scombrus* display mainly the presence of C, O and N in the eye lenses and Ca and P signatures in the exoccipital, the dentary and the basihyal (Electronic Supplementary Material Figure S5).

3.2. Mineralogical Analysis of Triazeugacanthus Skeleton

The FTIR spectrum of *Triazeugacanthus* skeletal structures displays the characteristic absorption bands of apatite (Figure 6a–c) [28]. These bands are related to the internal vibrational modes of PO_4 groups. The phosphate groups lead to intense bands at 565–576 and 605 cm^{-1} (PO_4 bending modes), and 1041 and 1096 cm^{-1} (PO_4 anti-symmetric stretching modes).

A weaker band related to the PO_4 symmetric stretching mode is observed at 965 cm^{-1}. The wavenumber of this band is correlated with F concentration and ranges between 960 in modern fish bone [29] to 965.6 cm^{-1} in a sedimentary carbonate-fluorapatite [28]. Its position in the present study thus corroborates the presence of a F concentration in apatite, consistent with the EDX measurements performed on specific skeletal structures of *Triazeugacanthus* (Figure 2i–n). The width of this band is dominated by the atomic-scale distortions of the apatite-structure [30] but overlapping with the strong PO_4 anti-symmetric stretching bands affects accurate analysis.

The splitting factor (IRSF) determined from the relative intensity of PO_4 bending bands is a practical way to assess the width of these bands, which is expected to reflect the apatite crystalline order but may also depend on the shape of apatite particles (Figure 6b). However, for samples with ordinary particle shapes, the full width at half maximum (FWMH) of the PO_4 symmetric stretching band and the infrared splitting factor (IRSF) parameter lead to similar information about apatite crystalline order [28]. In the present sample, the IRSF is 5.17, notably higher than that previously reported for bioapatite and slightly smaller than that reported for a sedimentary carbonate-fluorapatite sample [28]. For example, an IRSF of ~2.8 has been reported for vertebral centra of modern shark and ranging between 3.41 and 5.39 for Cenozoic fossil sharks [31,32]. Values of 2.6 and 3.2 have been reported for newly formed bones (fin rays) in the extant zebrafish *Danio rerio* [15]. Recent marine apatites also display low IRSF indices (3.0–3.6), whereas those of inland ancient apatites are higher (4.5–7.8) [26]. The IRSF of extant mammal bones exposed on tropical savannah grasslands varies from 2.7 to 3.5 and was found to be correlated to the mean length of apatite particles [33]. IRSF values increase to approximately 3.9 in Pleistocene bird and mammal bones [9]. The enamel of modern mammals displays a relatively high IRSF (e.g., 4.3 [24]). The comparatively high IRSF of *Triazeugacanthus* skeletal structures suggests that diagenetic transformations increased the apatite crystalline order with respect to that observed in extant and extinct biological materials.

Several bands related to vibrational modes of carbonate groups are also observed. Carbonate groups are responsible for the set of absorption bands at 1426 and 1453 cm^{-1} (anti-symmetric stretching) and the two overlapping signals at 865 and 874.4 cm^{-1} (out-of-plane bending modes). An additional band at 712 cm^{-1} indicates the presence of calcite.

Based on the signal related to out-of-plane bending modes, two main environments of carbonate groups occur in the sample. The band at 875 cm^{-1} can be mostly ascribed to calcite. The band at 865 cm^{-1} is related to carbonate groups incorporated in the apatite structure with a "francolite"-type environment [34]. This peculiar environment corresponds to an isovalent coupled substitution of the phosphate groups by clumped carbonate and F ions. Note that this type of environment does not imply any bonded interaction between the carbonate and the F ions but corresponds to a geometrical association, which ensures a local electrostatic charge neutrality.

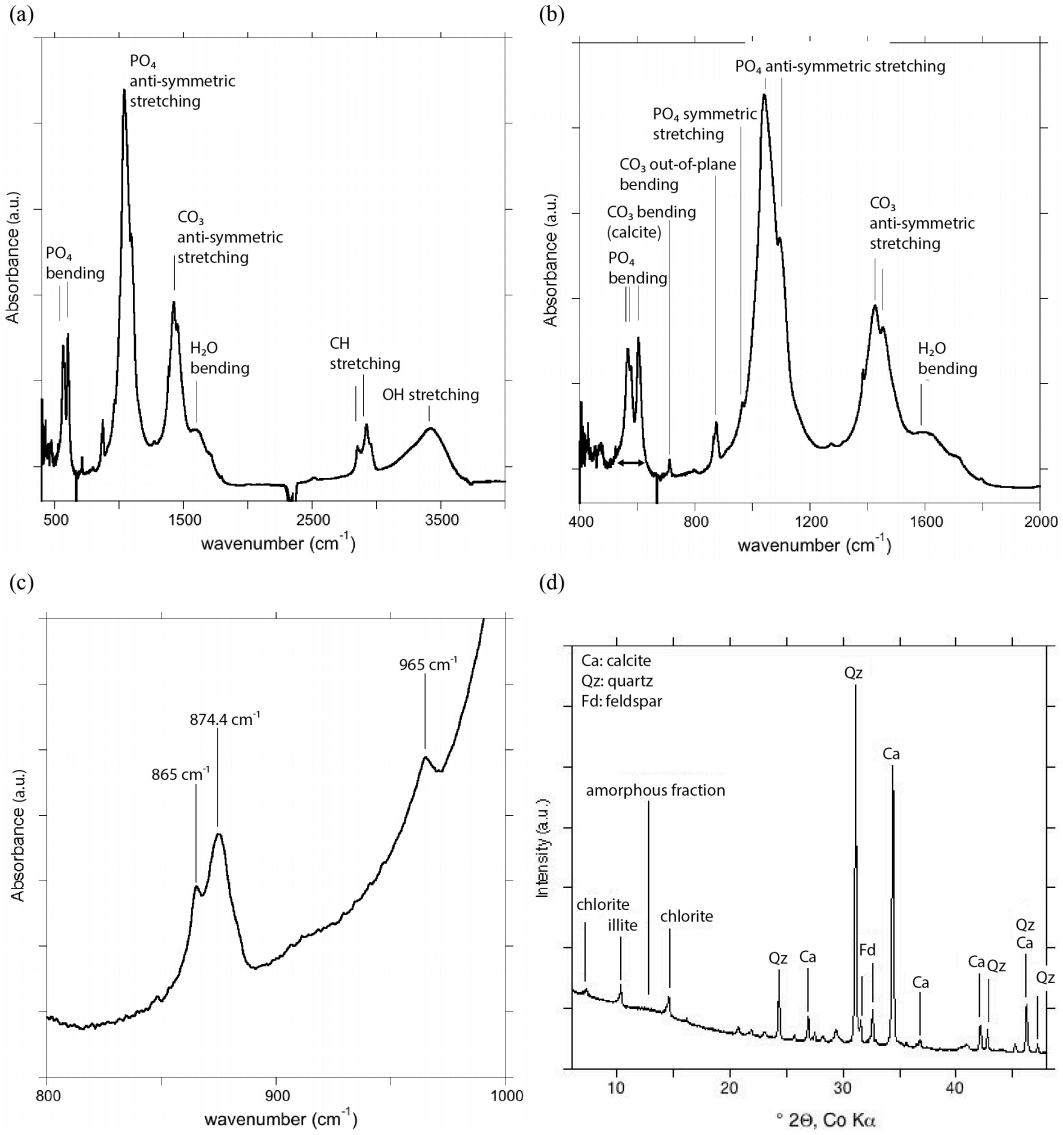

Figure 6. Powder transmission infrared spectrum of *Triazeugacanthus* and X-ray diffraction (XRD) pattern of surrounding sedimentary matrix. (**a**) Powder transmission infrared spectrum of *Triazeugacanthus* (MHNM 03-1699) showing PO_4, CO_3, OH, CH and H_2O bands and close-up (**b**) focusing on major CO_3 and PO_4 bands. Horizontal arrow points the line splitting of PO_4 bending modes. (**c**) Close-up of the Fourier transform infrared spectrometry (FTIR) spectrum focusing on the ν_2 CO_3 and ν_1 PO_4 signals. The band at 865 cm^{-1} is diagnostic of the presence of a francolite-type carbonate environment. (**d**) XRD pattern of sedimentary matrix surrounding the specimen of *Triazeugacanthus*.

The absorption bands related to the two anti-symmetric stretching modes of CO_3 groups, split by the site distortion, are observed at 1409–1440 cm^{-1} and 1450–1455 cm^{-1} (Figure 6b). These

frequencies are consistent with the above interpretation. The absence of a marked absorption band at higher frequency (1550 cm^{-1}) rules out a major occurrence of carbonate groups in the structural channels of apatite (A-type carbonates). However, an uncertainty remains about the occurrence of carbonate groups in the usual B-type environment of hydroxyapatite because of its potential overlap with the calcite and "francolite"-type carbonate bands. The peculiar "francolite"-type substitution at the B-site of fluorapatite differs from ordinary B-type carbonate substitution. In biological apatite, the B-type carbonate substitution corresponds to the replacement of PO_4^{3-} by CO_3^{2-}, along with the substitution of Ca^{2+} by Na^+ or K^+ to preserve the electroneutrality.

Broad absorption features between 1560 and 1800 cm^{-1} are related to the presence of organic matter (carbonyl and amide functions) and water molecules (H_2O bending mode). Water molecules are also responsible for the broad OH-stretching band at 3420 cm^{-1}. In contrast, no stretching band related to OH groups in the structural channels of hydroxyapatite (at 3572 cm^{-1}) is observed.

Taken together, these results indicate that the mineral composition of the fossilized *Triazeugacanthus* skeleton mostly consists of carbonate-fluorapatite and calcite. As bioapatite usually consists in poorly ordered carbonate-bearing hydroxyapatite, the occurrence of carbonate-fluorapatite strongly suggests a post-depositional recrystallisation of the bioapatite [26].

Finally, the sedimentary matrix surrounding the fossil sample was analyzed by X-ray diffraction to better infer the conditions of preservation of *Triazeugacanthus* fossils (Electronic Supplementary Material Figure S1). The observed minerals are dominantly calcite and quartz with feldspar, chlorite and illite in lower abundance (Figure 6d). Note that the clay fraction could also contain smectite but its identification would require further physical separation and chemical treatments because of the overlap of the smectite with the chlorite (001) peak. The presence of an amorphous fraction is suggested by a weak broad band at 12° in the diffraction pattern (Figure 6d). Overall, these results are consistent with previously published data [35,36] showing the occurrence of quartz, calcite and smaller proportions of illite, muscovite, chlorite, plagioclase and amorphous organic matter. This mineralogical composition has been interpreted as resulting from shallow burial diagenesis and early formation of diagenetic calcite [35,36].

4. Discussion

Here, we have shown that (1) both unmineralized (carbon signature) and mineralized anatomical elements (calcium and phosphorus signatures) are preserved depending on the ontogenetic stages of *Triazeugacanthus*; and (2) the carbonate-fluorapatite is the main mineralogical structure of *Triazeugacanthus* fossil skeleton.

4.1. Chemical Composition of Triazeugacanthus Biomineralized Tissues Depends on Ontogenetic Stages

Published spectrometry on *Triazeugacanthus* reported the dominant presence of Si with traces of Al, K, Mg, Ca and Fe for various skeletal elements (scales, “vertebral column” and “adjacent plates”) [37]. Our observations do not confirm this previous report, which may correspond to an analytical artifact. It is unlikely that the specimen used for that study [37] would be indicative of silicification, while none of our specimens show such a chemical signature.

Our results indicate that both unmineralized (C signature) and mineralized anatomical remains (Ca and P signatures) are preserved differentially according to the ontogenetic stages of *Triazeugacanthus* and the histological origin of the elements. With the exception of the notochordal elements for which a non-mineralized signature has been found in the immatures, the pre-mineralized (cartilaginous) state of endochondral elements has not been observed in our coarse sampling of the ontogenetic series of *Triazeugacanthus*. The notochordal elements correspond either to the cartilaginous precursors of vertebral elements or to the notochord itself. The appearance and growth of dermal elements is always characterized by the presence of both Ca and P peaks. However, a difference has been noticed between the elemental composition at the surface of the bone and the

internal structure of the bone; F has been recorded at the exposed surface (scales and spines), while it is not recorded internally.

While the larval individuals show the preservation of soft tissues (e.g., eye lenses, notochordal elements), juveniles and adults display notable concentrations of Ca and P, which are characteristic of bone chemical composition [38]. However, in the juveniles, the relative P/Ca content in the scales and fin spines is smaller than in the adults. Therefore, we interpret this progressive mineralization of skeletal elements as reflecting an ontogenetic transformation of the bony material.

EDX analyses and anatomical comparisons allowed us to identify properly the rounded anteriormost elements observed in the head of *Triazeugacanthus* (Figure 1a,b) [37,39,40]. These elements have been alternately interpreted as (1) optic plates [37]; (2) orbits [40]; and (3) eye lenses [21]. The use of the term "optic plates" was not justified in the original paper [37], as this term does not correspond to any anatomical element. The term "orbit" (="orbital cavity" [41]) corresponds either to the cavity that structurally supports the eyeball, or the bones (e.g., circumorbitals) forming the margin of the eye socket [42]. None of the known acanthodian neurocrania [43,44] display paired rounded elements as those seen in *Triazeugacanthus*. A series of four dermal sclerotic plates forms the margin of the eye socket of *Triazeugacanthus* (this study, [40,42]). Thus, the rounded elements seen in *Triazeugacanthus* do not correspond to the orbit. Anterior paired rounded elements have been identified as the eyes of the Carboniferous acanthodian *Acanthodes bridgei* [45]. Rods and pigments, as well as molecules common only to eumelanine, were found in the dark brown fragments from these fossil eyes. EDX analyses on the eye lenses of the extant *C. fabricii* and *S. scombrus* are similar to those of the *Triazeugacanthus* elements (this study). Characteristics of the crystalline lens of aquatic vertebrates (e.g., rounded-shape of the lens with low deformability [46]) and similarities shared with cartilage (abundance and chemical composition of crystalline proteins and collagen proteins [47] in the lens and the cartilage, respectively) might explain its potential for fossilization. We suggested that the rounded elements in *Triazeugacanthus* specimens could be interpreted as eye lenses. The anterior morphological position in the head region, their rounded shape, the absence of mineralized tissues (C and O peaks), and the similarities with acanthodian, chondrichthyan and osteichthyan anatomy (this study, [45]) corroborate this interpretation.

4.2. Preservation versus Recrystallization of Triazeugacanthus Tissues

In the stratigraphic sequence of the Miguasha *Fossil-Lagerstätte*, larval, juvenile and adult *Triazeugacanthus* are found in the same lithologies, primarily in laminites, as well as on the same bedding plane. The characteristic "laminites" facies is composed of an alternation of fine siltstones and shales [22] rich in organic matter interpreted as a tidal deposit [35]. This lithofacies is in agreement with an intertidal deposit likely in a wave-dominated estuarine environment, with periodic input of sediment by floods [22]. Miguasha *Konservat-* and *Konzentrat-Lagerstätte* horizons occur mostly in the transgressive phases and primarily towards the maximum paleodepth water [22]. Sedimentological and geochemical investigations have shown that the Escuminac Formation has been subjected only to a shallow burial diagenesis (depth < 1500 m, T < 430 °C) [35,36,48]. The clay mineral fraction is considered to be mostly detrital whereas calcite cement and fibrous calcite are attributed to early diagenesis of organic matter [35]. Thus, shallow burial allowing exchanges between groundwater and skeleton, and early diagenesis are required conditions for recrystallization of skeletal structures.

Despite the excellent state of preservation of bones at the microstructural [49–51], histological (Figure 1h,i) and anatomical levels, our results indicate a pervasive recrystallization of bioapatite in *Triazeugacanthus* skeletal structures. Modification of the mineral composition of fossil bones (e.g., presence of authigenic calcite) from the Escuminac Formation has been previously reported in the placoderm *Bothriolepis canadensis* and the osteolepiform *Eusthenopteron foordi* [36]. Bioapatites usually display small particle sizes and significant carbonate contents [15,52]. In addition, apatite particles in bones of living animals are coated by a poorly-ordered hydrous phosphatic phase [53]

and associated with organic polymers (collagen), which transform [54] or decay after an animal's death [55]. In contrast, carbonate-fluorapatite is less soluble than bioapatite [26,54] and often represents an ultimate stage of recrystallization of biomineralized anatomical structures in geological environments [26,28,52,54,56]. Carbonate-fluorapatite also occurs in sedimentary environments as an authigenic mineral, likely produced from the bacterial decay of organic matter [57–60].

Transformation of bioapatite to carbonate-fluorapatite can occur in low-temperature environments and has been reported in marine or continental fossil deposits [14,28,52,61]. It however depends on the F supply. In the present case, the F source might be related to the early diagenetic transformation of carbonates. As a matter of fact, the early diagenesis of biogenic calcium carbonate minerals has been reported to be a major source of F in modern shallow sediments of the Florida Bay, USA [62]. The transformation of bioapatite in carbonate-bearing fluroapatite is, thus, still consistent with the rapid burial and early diagenetic transformations under anoxic conditions. Indeed, rapid burial and early diagenetic transformations limiting the rapidity of consumption and degradation, which are the most important bias in the preservation of soft tissues, allowed the preservation of these tissues such as those observed in *Triazeugacanthus* larvae [17,63].

Finally, bioapatite to carbonate-fluorapatite transformation of mammal enamel in late Tertiary continental environments has been shown to occur through a dissolution/precipitation mechanism [28]. However, such type of replacement modifies the structure of the biological material at a micrometric scale (e.g., presence of carbonate-fluorapatite infillings discordant with the biogenic Retzius striae in mammalian tooth enamel [28]). In the Miguasha *Fossil-Lagerstätte*, the preservation of the bone microstructures [49–51,64] could suggest a more subtle transformation mechanism, consistent with an early diagenetic stage, even though the formation of the "francolite"-type environment of substituted carbonates implies a transformation of apatite down to the atomic scale. Therefore, the respective contributions of early transformation and potential slow modifications [65] in the sedimentological environment of the Escuminac Formation have still to be determined.

5. Concluding Remarks

The preservation of fossil anatomical remains, especially the preservation of soft tissues, and pervasive chemical modification of hard tissues in the same sedimentary horizons, suggest specific conditions of burial and diagenesis. The investigation of ontogenetic changes of the Late Devonian acanthodian *Triazeugacanthus affinis*, using different methods for chemical identification, allowed us to better describe the growth in this fossil fish in documenting the progressive mineralization. The presence of soft tissues in larvae and the biomineralization of tissues in juveniles and adults throughout a growth series are described for the first time in a Paleozoic vertebrate.

Supplementary Materials: The following are available online at www.mdpi.com/2075-163X/6/1/1/s1.

Acknowledgments: For the access to collections, we thank Johanne Kerr, Olivier Matton and France Charest (MHNM). We thank Claude Belzile (UQAR) for scanning electron microscopy (SEM) and EDX analyses. We thank members of the Maurice Lamontagne Institute (DFO-MPO) for providing us with juvenile specimens of living fishes. Cyrena Riley (UQAR) helped with the preparation of the black dogfish specimen. François Grégoire (UQAR) provided juvenile mackerels. We are grateful to Maxime Guillaumet (IMPMC), Benoit Baptiste (IMPMC) and Guillaume Morin (IMPMC) for their help in FTIR and XRD measurements. This project was supported financially by NSERC Discovery grant (RC), UQAR Research Chair in Paleontology and Evolutionary Biology (RC), EnviroNorth mobility grant (MC), and the team “Evolution et développement du squelette” (CNRS, IPBS Paris). We also thank the Labex Matisse for organizing the biomineralization short course and proposing this special issue.

Author Contributions: Marion Chevrinais, Etienne Balan and Richard Cloutier conceived and designed the experiments; Marion Chevrinais and Etienne Balan performed the analyses; Marion Chevrinais, Etienne Balan and Richard Cloutier analyzed the data; Marion Chevrinais and Etienne Balan conceived the figures; Marion Chevrinais wrote the first version of the paper; all authors contributed to the final version.

Conflicts of Interest: The authors declare no conflict of interest.

References

1. Cloutier, R. The fossil record of fish ontogenies: Insights into developmental patterns and processes. *Semin. Cell Dev. Biol.* **2010**, *21*, 400–413. [CrossRef] [PubMed]
2. Donoghue, P.C.J.; Sansom, I.J. Origin and early evolution of vertebrate skeletonization. *Microsc. Res. Tech.* **2002**, *59*, 352–372. [CrossRef] [PubMed]
3. Kemp, N.E.; Westrin, S.K. Ultrastructure of calcified cartilage in the endoskeletal tesserae of sharks. *J. Morphol.* **1979**, *160*, 75–101. [CrossRef] [PubMed]
4. Dean, M.N.; Summers, A.P. Mineralized cartilage in the skeleton of chondrichthyan fishes. *Zoology* **2006**, *109*, 164–168. [CrossRef] [PubMed]
5. Grünbaum, T.; Cloutier, R.; Vincent, B. Dynamic skeletogenesis in fishes: Insight of exercise training on developmental plasticity. *Dev. Dyn.* **2012**, *241*, 1507–1524. [CrossRef] [PubMed]
6. Faustino, M.; Power, D.M. Osteologic development of the viscerocranial skeleton in sea bream: Alternative ossification strategies in teleost fish. *J. Fish Biol.* **2001**, *58*, 537–572. [CrossRef]
7. Gavaia, P.J.; Sarasquete, C.; Cancela, M.L. Detection of mineralized structures in early stages of development of marine Teleostei using a modified alcian blue-alizarin red double staining technique for bone and cartilage. *Biotech. Histochem.* **2000**, *75*, 79–84. [CrossRef] [PubMed]
8. Johanson, Z.; Trinajstic, K. Fossilized ontogenies: The contribution of placoderm ontogeny to our understanding of the evolution of early gnathostomes. *Palaeontology* **2014**, *57*, 505–516. [CrossRef]
9. Trueman, C.N.; Privat, K.; Field, J. Why do crystallinity values fail to predict the extent of diagenetic alteration of bone mineral? *Palaeogeogr. Palaeoclimatol. Palaeoecol.* **2008**, *266*, 160–167. [CrossRef]
10. Morris, S.C.; Caron, J.-B. *Pikaia gracilens* Walcott, a stem-group chordate from the Middle Cambrian of British Columbia. *Biol. Rev.* **2012**, *87*, 480–512. [CrossRef] [PubMed]
11. Arsenault, M.; Desbiens, S.; Janvier, P.; Kerr, J. New data on the soft tissues and external morphology of the antiarch *Bothriolepis canadensis* (Whiteaves, 1880), from the Upper Devonian of Miguasha, Quebec. In *Recent Advances in the Origin and Early Radiation of Vertebrates*; Arratia, G., Wilson, M.V.H., Cloutier, R., Eds.; Verlag Dr. Friedrich Pfeil: München, Germany, 2004; pp. 439–454.
12. Trinajstic, K.; Marshall, C.; Long, J.; Bifield, K. Exceptional preservation of nerve and muscle tissues in Late Devonian placoderm fish and their evolutionary implications. *Biol. Lett.* **2007**, *3*, 197–200. [CrossRef] [PubMed]
13. Cloutier, R. Great Canadian *Lagerstätten* 4. The Devonian Miguasha biota (Québec): UNESCO World Heritage Site and a time capsule in the early history of vertebrates. *Geosci. Can.* **2013**, *40*, 149–163. [CrossRef]
14. Kolodny, Y.; Luz, B.; Sander, M.; Clemens, W.A. Dinosaur bones: Fossils or pseudomorphs? The pitfalls of physiology reconstruction from apatitic fossils. *Palaeogeogr. Palaeoclimatol. Palaeoecol.* **1996**, *126*, 161–171. [CrossRef]
15. Mahamid, J.; Sharir, A.; Addadi, L.; Weiner, S. Amorphous calcium phosphate is a major component of the forming fin bones of zebrafish: Indications for an amorphous precursor phase. *Proc. Natl. Acad. Sci.* **2008**, *105*, 12748–12753. [CrossRef] [PubMed]
16. Cambra-Moo, O.; Nacarino-Meneses, C.; Díaz-Güemes, I.; Enciso, S.; Gil, O.G.; Rodríguez, L.L.; Barbero, M.Á.R.; Antonio, H.; Martín, A.G. Multidisciplinary characterization of the long-bone cortex growth patterns through sheep's ontogeny. *J. Struct. Biol.* **2015**, *191*, 1–9. [CrossRef] [PubMed]
17. Allison, P.A.; Briggs, D.E.G. Taphonomy of Nonmineralized Tissues. In *Taphonomy: Releasing the Data Locked in the Fossil Record*; Allison, P.A., Briggs, D.E.G., Eds.; Plenum Press: New York, NY, USA, 1991; Volume 9.
18. Schopf, J.M. Modes of fossil preservation. *Rev. Palaeobot. Palynol.* **1975**, *20*, 27–53. [CrossRef]
19. Briggs, D.E.G. The role of decay and mineralization in the preservation of soft-bodied fossils. *Annu. Rev. Earth Planet. Sci.* **2003**, *31*, 275–301. [CrossRef]
20. Cloutier, R.; Béchard, I.; Charest, F.; Matton, O. La contribution des poissons fossiles du parc national de Miguasha à la biologsie évolutive du développement. *Nat. Can.* **2009**, *133*, 84–95. (In French).
21. Chevrinais, M.; Cloutier, R.; Sire, J.-Y. The revival of a so-called rotten fish: The ontogeny of the Devonian acanthodian *Triazeugacanthus*. *Biol. Lett.* **2015**, *11*. [CrossRef] [PubMed]
22. Cloutier, R.; Proust, J.-N.; Tessier, B. The Miguasha Fossil-Fish-Lagerstätte: A consequence of the Devonian land-sea interactions. *Palaeobiodivers. Palaeoenviron.* **2011**, *91*, 293–323. [CrossRef]

23. Gupta, N.S.; Cambra-Moo, O.; Briggs, D.E.G.; Love, G.D.; Fregenal-Martinez, M.A.; Summons, R.E. Molecular taphonomy of macrofossils from the Cretaceous Las Hoyas Formation, Spain. *Cretac. Res.* **2008**, *29*, 1–8. [CrossRef]
24. Schweitzer, M.H.; Avci, R.; Collier, T.; Goodwin, M.B. Microscopic, chemical and molecular methods for examining fossil preservation. *Comptes Rendus Palevol* **2008**, *7*, 159–184. [CrossRef]
25. Weiner, S.; Bar-Yosef, O. States of preservation of bones from prehistoric sites in the Near East: A survey. *J. Archaeol. Sci.* **1990**, *17*, 187–196. [CrossRef]
26. Shemesh, A. Crystallinity and diagenesis of sedimentary apatites. *Geochim. Cosmochim. Acta* **1990**, *54*, 2433–2438. [CrossRef]
27. Schultze, H.-P. A new acanthodian from the Pennsylvanian of Utah, USA, and the distribution of otoliths in gnathostomes. *J. Vertebr. Paleontol.* **1990**, *10*, 49–58. [CrossRef]
28. Yi, H.; Balan, E.; Gervais, C.; Ségalen, L.; Roche, D.; Person, A.; Fayon, F.; Morin, G.; Babonneau, F. Probing atomic scale transformation of fossil dental enamel using Fourier transform infrared and nuclear magnetic resonance spectroscopy: A case study from the Tugen Hills (Rift Gregory, Kenya). *Acta Biomater.* **2014**, *10*, 3952–3958. [CrossRef] [PubMed]
29. Pucéat, E.; Reynard, B.; Lécuyer, C. Can crystallinity be used to determine the degree of chemical alteration of biogenic apatites? *Chem. Geol.* **2004**, *205*, 83–97. [CrossRef]
30. Balan, E.; Delattre, S.; Roche, D.; Segalen, L.; Morin, G.; Guillaumet, M.; Blanchard, M.; Lazzeri, M.; Brouder, C.; Salje, E.K.H. Line-broadening effects in the powder infrared spectrum of apatite. *Phys. Chem. Miner.* **2011**, *38*, 111–122. [CrossRef]
31. MacFadden, B.J.; Labs-Hochstein, J.; Quitmyer, I.; Jones, D.S. Incremental growth and diagenesis of skeletal parts of the lamnoid shark *Otodus obliquus* from the early Eocene (Ypresian) of Morocco. *Palaeogeogr. Palaeoclimatol. Palaeoecol.* **2004**, *206*, 179–192. [CrossRef]
32. Labs-Hochstein, J.; MacFadden, B.J. Quantification of diagenesis in Cenozoic sharks: Elemental and mineralogical changes. *Geochim. Cosmochim. Acta* **2006**, *70*, 4921–4932. [CrossRef]
33. Trueman, C.N.G.; Behrensmeyer, A.K.; Tuross, N.; Weiner, S. Mineralogical and compositional changes in bones exposed on soil surfaces in Amboseli National Park, Kenya: Diagenetic mechanisms and the role of sediment pore fluids. *J. Archaeol. Sci.* **2004**, *31*, 721–739. [CrossRef]
34. Yi, H.; Balan, E.; Gervais, C.; Segalen, L.; Fayon, F.; Roche, D.; Person, A.; Morin, G.; Guillaumet, M.; Blanchard, M. A carbonate-fluoride defect model for carbonate-rich fluorapatite. *Am. Mineral.* **2013**, *98*, 1066–1069. [CrossRef]
35. El Albani, A.; Cloutier, R.; Candilier, A.-M. Early diagenesis of the Upper Devonian Escuminac Formation in the Gaspé Peninsula, Québec: Sedimentological and geochemical evidence. *Sediment. Geol.* **2002**, *146*, 209–223. [CrossRef]
36. Matton, O.; Cloutier, R.; Stevenson, R. Apatite for destruction: Isotopic and geochemical analyses of bioapatites and sediments from the Upper Devonian Escuminac Formation (Miguasha, Québec). *Palaeogeogr. Palaeoclimatol. Palaeoecol.* **2012**, *361*, 73–83. [CrossRef]
37. Béland, P.; Arsenault, M. Scauménellisation de l'Acanthodii *Triazeugacanthus affinis* (Whiteaves) de la Formation d'Escuminac (Dévonien supérieur de Miguasha, Québec): Révision du *Scaumenella mesacanthi* Graham-Smith. *Can. J. Earth Sci.* **1985**, *22*, 514–524. (In French).
38. Young, R.A.; Brown, W.E. Structures of Biological Minerals. In *Biological Mineralization and Demineralization*; Springer: Berlin, Germany, 1982; pp. 101–141.
39. Graham-Smith, W. *Scaumenella mesacanthi*, gen. et sp. n., a peculiar organism from the Upper Devonian of Scaumenac Bay, Province Quebec, Canada. *Ann. Mag. Nat. Hist.* **1935**, *16*, 473–476. [CrossRef]
40. Gagnier, P.-Y. Acanthodii. In *Devonian Fishes and Plants of Miguasha, Quebec, Canada*; Schultze, H.-P., Cloutier, R., Eds.; Verlag Dr. Friedrich Pfeil: München, Germany, 1996; pp. 149–164.
41. Franz-Odendaal, T.A.; Vickaryous, M.K. Skeletal elements in the vertebrate eye and adnexa: Morphological and developmental perspectives. *Dev. Dyn.* **2006**, *235*, 1244–1255. [CrossRef] [PubMed]
42. Burrow, C.J.; Newman, M.J.; Davidson, R.G.; Den Blaauwen, J.L. Sclerotic plates or circumorbital bones in early jawed fishes? *Palaeontology* **2011**, *54*, 207–214. [CrossRef]
43. Brazeau, M.D. The braincase and jaws of a Devonian "acanthodian" and modern gnathostome origins. *Nature* **2009**, *457*, 305–308. [CrossRef] [PubMed]

44. Davis, S.P.; Finarelli, J.A.; Coates, M.I. *Acanthodes* and shark-like conditions in the last common ancestor of modern gnathostomes. *Nature* **2012**, *486*, 247–250. [CrossRef] [PubMed]
45. Tanaka, G.; Parker, A.R.; Hasegawa, Y.; Siveter, D.J.; Yamamoto, R.; Miyashita, K.; Takahashi, Y.; Ito, S.; Wakamatsu, K.; Mukuda, T. Mineralized rods and cones suggest colour vision in a 300 Myr-old fossil fish. *Nat. Commun.* **2014**, *5*. [CrossRef] [PubMed]
46. Levine, J.S. The vertebrate eye. In *Functional Vertebrate Morphology*; Hildebrand, M., Bramble, D.M., Liem, K.F., Wake, D.B., Eds.; Harvard University Press: Cambridge, MA, USA, 1985; pp. 317–337.
47. Goodenough, D.A. The crystalline lens. A system networked by gap junctional intercellular communication. *Semin. Cell Biol.* **1992**, *3*, 49–58. [CrossRef]
48. Chidiac, Y. Paleoenvironmental interpretation of the Escuminac Formation based on geochemical evidence. In *Devonian Fishes and Plants of Miguasha, Quebec, Canada*; Schultze, H.P., Cloutier, R., Eds.; Verlag Dr Friedrich Pfeil: München, Germany, 1996; pp. 47–53.
49. Sanchez, S.; Dupret, V.; Tafforeau, P.; Trinajstic, K.M.; Ryll, B.; Gouttenoire, P.-J.; Wretman, L.; Zylberberg, L.; Peyrin, F.; Ahlberg, P.E. 3D microstructural architecture of muscle attachments in extant and fossil vertebrates revealed by synchrotron microtomography. *PLoS One* **2013**, *8*. [CrossRef] [PubMed]
50. Sanchez, S.; Tafforeau, P.; Ahlberg, P.E. The humerus of *Eusthenopteron*: A puzzling organization presaging the establishment of tetrapod limb bone marrow. *Proc. R. Soc. B Biol. Sci.* **2014**, *281*. [CrossRef] [PubMed]
51. Downs, J.P.; Donoghue, P.C.J. Skeletal histology of *Bothriolepis canadensis* (Placodermi, Antiarchi) and evolution of the skeleton at the origin of jawed vertebrates. *J. Morphol.* **2009**, *270*, 1364–1380. [CrossRef] [PubMed]
52. Nemliher, J.G.; Baturin, G.N.; Kallaste, T.E.; Murdmaa, I.O. Transformation of hydroxyapatite of bone phosphate from the ocean bottom during fossilization. *Lithol. Miner. Resour.* **2004**, *39*, 468–479. [CrossRef]
53. Wang, Y.; Von Euw, S.; Fernandes, F.M.; Cassaignon, S.; Selmane, M.; Laurent, G.; Pehau-Arnaudet, G.; Coelho, C.; Bonhomme-Coury, L.; Giraud-Guille, M.-M.; *et al*. Water-mediated structuring of bone apatite. *Nat. Mater.* **2013**, *12*, 1144–1153. [CrossRef] [PubMed]
54. Kalvoda, J.; Novák, M.; Bábek, O.; Brzobohatý, R.; Holá, M.; Holoubek, I.; Kanický, V.; Škoda, R. Compositional changes in fish scale hydroxylapatite during early diagenesis; an example from an abandoned meander. *Biogeochemistry* **2009**, *94*, 197–215. [CrossRef]
55. Sansom, R.S.; Gabbott, S.E.; Purnell, M.A. Atlas of vertebrate decay: A visual and taphonomic guide to fossil interpretation. *Palaeontology* **2013**, *56*, 457–474. [CrossRef]
56. Pasteris, J.D.; Ding, D.Y. Experimental fluoridation of nanocrystalline apatite. *Am. Mineral.* **2009**, *94*, 53–63. [CrossRef]
57. Cosmidis, J.; Benzerara, K.; Menguy, N.; Arning, E. Microscopy evidence of bacterial microfossils in phosphorite crusts of the Peruvian shelf: Implications for phosphogenesis mechanisms. *Chem. Geol.* **2013**, *359*, 10–22. [CrossRef]
58. Cosmidis, J.; Benzerara, K.; Gheerbrant, E.; Estève, I.; Bouya, B.; Amaghzaz, M. Nanometer-scale characterization of exceptionally preserved bacterial fossils in Paleocene phosphorites from Ouled Abdoun (Morocco). *Geobiology* **2013**, *11*, 139–153. [CrossRef] [PubMed]
59. O'Hagan, D.; Harper, D.B. Fluorine-containing natural products. *J. Fluor. Chem.* **1999**, *100*, 127–133. [CrossRef]
60. Murphy, C.D.; Schaffrath, C.; O'Hagan, D. Fluorinated natural products: The biosynthesis of fluoroacetate and 4-fluorothreonine in *Streptomyces cattleya*. *Chemosphere* **2003**, *52*, 455–461. [CrossRef]
61. Ifrim, C.; Stinnesbeck, W.; Frey, E. Upper Cretaceous (Cenomanian-Turonian and Turonian-Coniacian) open marine plattenkalk deposits in NE Mexico. *Neues Jahrb. Geol. Paläontol. Abh.* **2007**, *245*, 71–81. [CrossRef]
62. Rude, P.D.; Aller, R.C. Fluorine mobility during early diagenesis of carbonate sediment: An indicator of mineral transformations. *Geochim. Cosmochim. Acta* **1991**, *55*, 2491–2509. [CrossRef]
63. Allison, P.A. The role of anoxia in the decay and mineralization of proteinaceous macro-fossils. *Paleobiology* **1988**, *14*, 139–154.

64. Zylberberg, L.; Meunier, F.J.; Laurin, M. A microanatomical and histological study of the postcranial dermal skeleton in the Devonian sarcopterygian *Eusthenopteron foordi*. *Acta Palaeontol. Pol.* **2010**, *55*, 459–470. [CrossRef]
65. Reynard, B.; Balter, V. Trace elements and their isotopes in bones and teeth: Diet, environments, diagenesis, and dating of archeological and paleontological samples. *Palaeogeogr. Palaeoclimatol. Palaeoecol.* **2014**, *416*, 4–16. [CrossRef]